

# Electronic transport through occupied and unoccupied states of an organic molecule on Au: Experiment and theory

Michael Toerker,\* Torsten Fritz, and Holger Proehl

*Institut für Angewandte Photophysik, Technische Universität Dresden, 01062 Dresden, Germany*

Rafael Gutierrez, Frank Großmann,† and Rüdiger Schmidt

*Institut für Theoretische Physik, Technische Universität Dresden, 01062 Dresden, Germany*

(Received 4 October 2001; revised manuscript received 11 March 2002; published 21 June 2002)

Scanning tunneling spectroscopy (STS) measurements on highly ordered double layers of the planar organic molecule hexa-*peri*-hexabenzocoronene ( $C_{42}H_{18}$ ) on Au(100) are presented and compared to a theoretical characterization of the electronic conductance based on a combination of the Landauer transport formalism with a density-functional-parametrized tight-binding scheme within the local density approximation (LDA). Tunneling spectroscopy data have been recorded within an extended voltage range of  $\pm 2.5$  V. In this *room temperature* STS experiment it was possible to derive not only the energetic positions of the frontier orbitals of a molecular species from tunneling spectroscopy but also the energies of the molecular states next to these frontier orbitals. To achieve a satisfactory agreement between experiment and theory a scaling parameter is necessary which compensates for the underestimation of the electronic energy gap in LDA.

DOI: 10.1103/PhysRevB.65.245422

PACS number(s): 73.40.Gk, 73.63.Rt, 81.15.Hi, 68.37.Ef

## I. INTRODUCTION

Currently, there is intense research activity in the field of highly ordered organic thin films<sup>1–6</sup> motivated by the promising physical and chemical properties of these novel materials.<sup>7</sup> Scanning probe microscopy offers the possibility of probing physical properties with high spatial resolution. In particular, scanning tunneling microscopy (STM) and scanning tunneling spectroscopy (STS) can be used to combine structural characterization with probing the electronic signature of the organic compounds on a molecular scale. Although a number of STS investigations on organic materials have been published in recent years, most of the authors observed electron transport only through the frontier orbitals of the organic species [i.e., through the highest occupied molecular orbital (HOMO) and the lowest unoccupied molecular orbital (LUMO)]. In particular, at room temperature the contributions of the second filled and second unfilled molecular orbitals to the tunneling current have been measured in only a few studies.<sup>8–10</sup> Large flat hydrocarbons like hexa-*peri*-hexabenzocoronene (HBC, structural formula shown in Fig. 1) are useful as relatively simple model compounds which have been shown to grow in large ordered domains and which have interesting electronic properties.<sup>11,12</sup> The growth of HBC and derivatives on different substrates like Au(111),<sup>13</sup> highly oriented pyrolytic graphite (HOPG), and metal dichalcogenides,<sup>14,15</sup> as well as scanning tunneling spectroscopy measurements of pure<sup>16</sup> and alkyl-substituted HBC (Ref. 17) have already been published.

Here, we report a combined experimental/theoretical study of STS measurements on highly ordered HBC double-layer films at a Au(100) surface. In contrast to previous STS measurements on HBC (Ref. 16 and 17) we present scanning tunneling spectroscopy results which have been recorded at *room temperature* within an extended voltage range of  $\pm 2.5$  V. This enables us to derive not only the energetic

positions of the frontier orbitals of a molecular species from tunneling spectroscopy but also the energies of the second filled and second empty molecular state. The sample surface was imaged in STM measurements. The high degree of order within the molecular film enabled us to record STS data for a stable well-defined tunnel junction. The normalized differential conductance curves obtained from the measured  $I-V$  data (which reveal four peaks in correspondence to the energetic positions of the four molecular states) are compared to theoretical calculations using different STM-tip geometries. The theoretical treatment is based on the Landauer approach to electronic transport combined with a tight-binding-like scheme,<sup>18,20,21</sup> based on a density functional (DFT) parametrization within the local density approximation (LDA) for characterizing the electronic structure of both the HBC molecule and the electrodes. A satisfactory agreement between experimental and theoretical conductance spectra can be achieved by introducing a scaling parameter which compensates for the underestimation of the HOMO–LUMO gap, a fact well-known in DFT on the LDA level.<sup>22–24</sup>

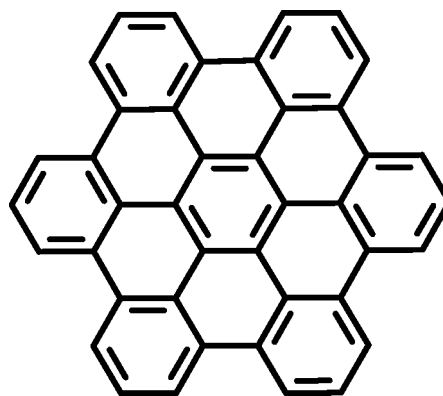


FIG. 1. Structural formula of hexa-*peri*-hexabenzocoronene ( $C_{42}H_{18}$ , HBC).

In Sec. II the experiments are described and the experimental results are presented. The theoretical approach is introduced in Sec. III. Finally, the theoretical results are discussed and compared to the experimental findings.

## II. EXPERIMENT

### A. Sample preparation and data processing

All experiments were carried out at room temperature and under ultrahigh vacuum (UHV) conditions in a three-chamber organic molecular beam epitaxy device (load lock, growth chamber, STM chamber) described in Ref. 13. A Au(100) single crystal was used as a substrate. This choice of crystal orientation was originally motivated by the question of whether the STS results are influenced by different molecular arrangements on Au(100) and Au(111), respectively. However, the STS results presented in this paper were obtained for approximately the same HBC lattice as in our previous study of HBC on Au(111),<sup>16</sup> but in contrast to this earlier study we have now been able to measure reproducible  $I$ - $V$  characteristics in an extended voltage range. Prior to deposition of HBC, the crystal was prepared by repeated cycles of argon ion bombardment [sputter ion source ISE 10 (Omicron), beam energy 600 eV, focus voltage 512 V, emission current 10 mA, sputter time 30 min, normal incidence] and subsequent annealing (870 K, 30 min). The Au(100) crystal was used for a number of deposition experiments. Before each experiment the surface was prepared by at least one sputter/annealing cycle. Annealing a HBC covered Au(100) crystal at 870 K without sputtering the surface before was not sufficient for the preparation of a clean gold surface: Deposition of HBC on the Au(100) crystal when it was just annealed after previous HBC film growth but not sputtered, did not result in the formation of ordered films. Residual HBC fragments are likely to be present on the surface when it is only annealed.

The annealing temperatures of the crystal and the tips, respectively, were measured using a thermocouple which was calibrated before by the use of an infrared radiation pyrometer and a test sample. The organic films were deposited by evaporation from low flux sublimation cells at a cell temperature of 675 K choosing a deposition time of 130 s. The deposition rate was about one monolayer (ML) per minute. The STM/STS measurements were carried out with a room-temperature UHV-STM system (Omicron STM/AFM) using two different types of tips: Tungsten tips were electrochemically etched from tungsten wire (0.25 mm in diameter) in NaOH solution and rinsed in distilled water and pure ethanol. Gold tips were simply cut from pure (99.99%) gold wire (0.25 mm in diameter). After transferring the tips into the vacuum system, all tips were annealed at about 870 K. Tungsten tips were also sputtered with 2-keV  $\text{Ar}^+$  ions to remove the oxide (focus voltage 512 V, emission current 10 mA, ion beam aligned with the tip axis, sputter time 20 min). Tunneling spectra were obtained in single point spectroscopy mode, i.e., the actual scan is stopped and the tip is moved to the desired position with the feedback loop closed, thereby adjusting the tip-sample distance. After a certain delay (100 ms) to allow for stabilization of the system, a voltage ramp

(step size 25 mV per 0.5 ms) is applied with the feedback loop being switched off. Each  $I$ - $V$  curve is averaged over two voltage sweeps ramping the bias voltage down and up, respectively. It was checked carefully that the averaging of the two  $I$ - $V$  curves did not produce any artificial structure in the spectra. There were also no limitations due to the dynamic range of the current amplifier for the data presented in this article. The bias voltage was applied to the sample in such a way that at positive voltages electrons tunnel from the tip to the substrate. For the interpretation of the spectroscopic data presented here, the normalized differential conductance of the measured  $I$ - $V$  curves  $[(dI/dV)/(I/V)]$  was calculated, which is known to be related to the density of states. This quantity was originally introduced by Feenstra, Stroscio, and Fein<sup>25</sup> for the discussion of STS experiments on inorganic semiconductor surfaces. Since then it has also been widely used for the interpretation of STS data measured on organic molecules.<sup>16,26-29</sup> For the calculation of the differential conductance the measured  $I$ - $V$  data were approximated stepwise by a polynomial fit. To avoid singularities in the normalized derivative  $(dI/dV)/(I/V)$  at  $V=0$ , we added a small constant to the value of  $I/V$  following the procedure of Prietsch *et al.*<sup>30</sup>

### B. Experimental results

A series of HBC on Au(100) samples with varying film thickness was investigated by STM and LEED (low energy electron diffraction). For deposition times of 60–70 s at the above-given cell temperature, the surface was uniformly covered by a less densely packed distorted hexagonal monolayer (lattice dimensions  $a=b=16.1$  Å,  $\angle(a,b)=62.2^\circ$ ). At this coverage one could switch between imaging the HBC lattice and the underlying Au(100) surface, respectively, simply by changing the tunneling parameters. At deposition times larger than 70 s the HBC structure changed to a densely packed true hexagonal phase ( $a=b=14.2$  Å,  $\angle(a,b)=60.0^\circ$ ). Unfortunately, it was not possible to obtain reproducible STS data for monolayer HBC films.

The monolayer growth scheme allows one to estimate the deposition time necessary for the growth of a 2-ML sample. In the case of nominally 2-ML coverage we were able to obtain reproducible STS data. Films thicker than nominally 2 ML have not been investigated. Figure 2(a) shows a 100 nm $\times$ 100 nm STM image of such a 2-ML film of HBC on Au(100). Steps of the underlying Au(100) surface are visible in the upper right-hand corner of the scan. With the exception of the single defect in the left part of the STM image, the surface is uniformly covered by the HBC film. Scanning other parts of the surface gave similar results. Figure 2(b) shows a 20 nm $\times$ 20 nm scan of a 2-ML HBC film imaged directly before recording the tunneling  $I$ - $V$  data presented in Fig. 3(a).

Tunneling spectroscopy measurements have been performed on highly ordered films of HBC on Au(100) of 2 ML thickness. A constant current STM image of such a sample is given in Fig. 2 showing the hexagonal arrangement of the molecules. This densely packed arrangement guarantees a high degree of stability of the film when moving the tip over

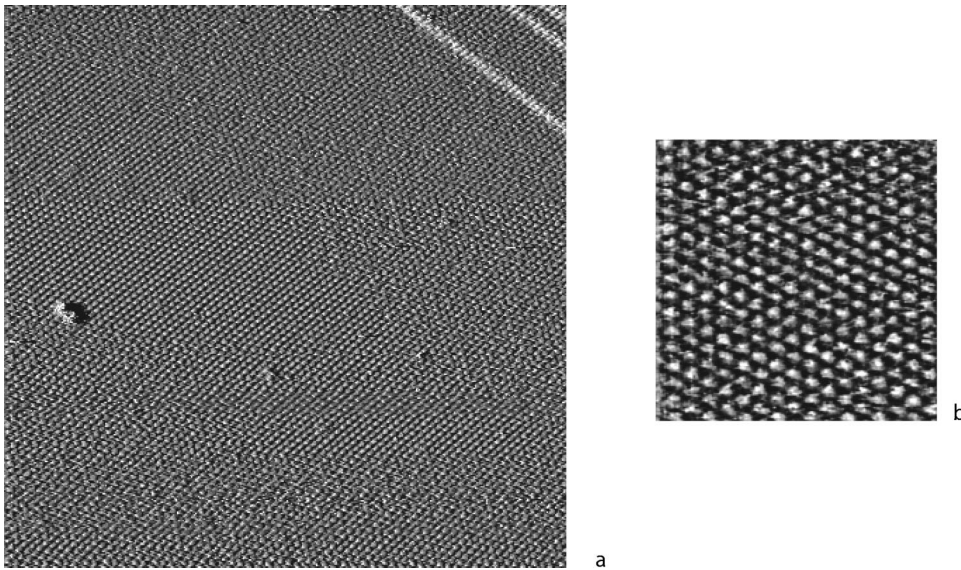


FIG. 2. (a) Constant height STM image of two monolayers of HBC on Au(100) (size=100 nm  $\times$  100 nm,  $V=0.65$  V,  $I=0.05$  nA). (b) Constant height STM image of a 2-ML HBC film imaged directly before recording the tunneling  $I-V$  data presented in Fig. 3(a) (size=20 nm  $\times$  20 nm,  $V=0.7$  V,  $I=0.05$  nA).

the sample surface and when recording the  $I-V$  data. Figure 3(a) shows two  $I-V$  curves measured for two different (fixed) tip-sample distances at the same lateral position. For this experiment a tungsten tip was used. The separation  $z_1$  is determined by the tunneling parameters, i.e., the tunneling current and the applied bias voltage, when the feedback loop is switched on. In the case of Fig. 3(a) these are 0.05 nA and 0.7 V, respectively, which were also typical parameters for imaging the sample. The corresponding normalized differential conductance curves presented in Fig. 3(b) reveal two peaks within the voltage region of  $-1.8$  to  $+2.0$  V. The peak positions are  $+1.8$  and  $-1.4$  V. Then, the tip-sample separation was increased by changing the  $z$  piezo-voltage when the feedback loop was open, i.e., the tip-sample separation is not only determined by the tunneling parameters before switching off the feedback loop but also by the change in the  $z$  piezo-voltage, leading to an increase in the gap distance by nominally  $2.5$  Å. At this larger separation, the applied voltage range could be extended to  $\pm 2.0$  V without overmodulation of the current preamplifier. Within this range three peak positions in the normalized differential conductance were found, with two peaks being identical to the positions at the smaller tip-sample separation (i.e.,  $+1.8$  and  $-1.4$  V). The third peak is observed at  $-2.0$  V. For better visibility, the two curves in Fig. 3(b) are vertically shifted relative to each other by an additive constant of 5. It is worthwhile to note that otherwise the two curves would nicely fall on top of each other due to the normalization applied, indicating that the normalized results are indeed independent of the actual sample-tip separation as expected if the results are thought to be related to the density of states.<sup>25</sup>

Recently we found that a modification of the data acquisition procedure allows us to extend the bias voltage range up to  $\pm 2.5$  V without amplifier overmodulation: the tunneling parameters were changed from 0.05 nA/0.7 V to 0.2 nA/ $-1.5$  V *before* performing the STS measurements (i.e., with the feedback loop being closed), thereby readjusting the tip-sample distance. The corresponding  $I-V$  curve is shown in Fig. 3(c). In this case the normalized differential

conductance [Fig. 3(d)] reveals four peaks. Besides the peaks at  $+1.8$ ,  $-1.4$ , and  $-2.0$  V, which are still clearly visible in the spectrum, an additional peak is now accessible at  $+2.2$  V. Again, due to the normalization, the results of this modified procedure nearly coincide in both energetic position and height with the former results shown in Fig. 3(b) in the common voltage range. This is even more remarkable considering the fact that the  $I-V$  curve in Fig. 3(c) was measured using a gold tip instead of a tungsten tip, proving that the results are indeed tip-independent. Furthermore, it also allows a direct comparison of the experimental data with the theory which assumes a tip consisting of gold atoms (see Sec. III).

STS results which were independent of the tip material were reported also for metal(II)-tetraphenylporphyrins on Au(111) using Pt/Ir- and tungsten tips.<sup>8</sup>

Before turning to the theoretical calculations the question of a potential drop at the molecule-substrate interface should be addressed. This problem was discussed in several publications.<sup>8,9,31-33</sup> Unlike other authors who considered such a bias-dependent potential drop in theoretical calculations<sup>31</sup> or used it as a fitting parameter when comparing calculated and experimentally obtained  $I-V$  curves,<sup>9,33</sup> we assume that in the case of HBC on Au(100) the applied potential is dropped entirely between the molecule and the tip. This assumption is supported by our recent ultraviolet photoelectron spectroscopy (UPS)/STS study of HBC on Au(111).<sup>16</sup> Therein, the HOMO position of HBC on Au(111) was derived from the STS measurements with the assumption that there is no voltage drop at the molecule-substrate interface. The thus obtained HOMO position was in perfect agreement with the value obtained in the UPS measurements, thereby justifying the assumption made. These observations are similar to the results of Scudiero *et al.*, who found excellent agreement between STS and UPS data for metal(II)-tetraphenylporphyrins on Au(111).<sup>8</sup>

Another finding supporting the absence of a bias-dependent potential drop at the molecule-substrate interface is that the peak positions in the curves in Fig. 3(b) are identical, although the two curves were measured for different

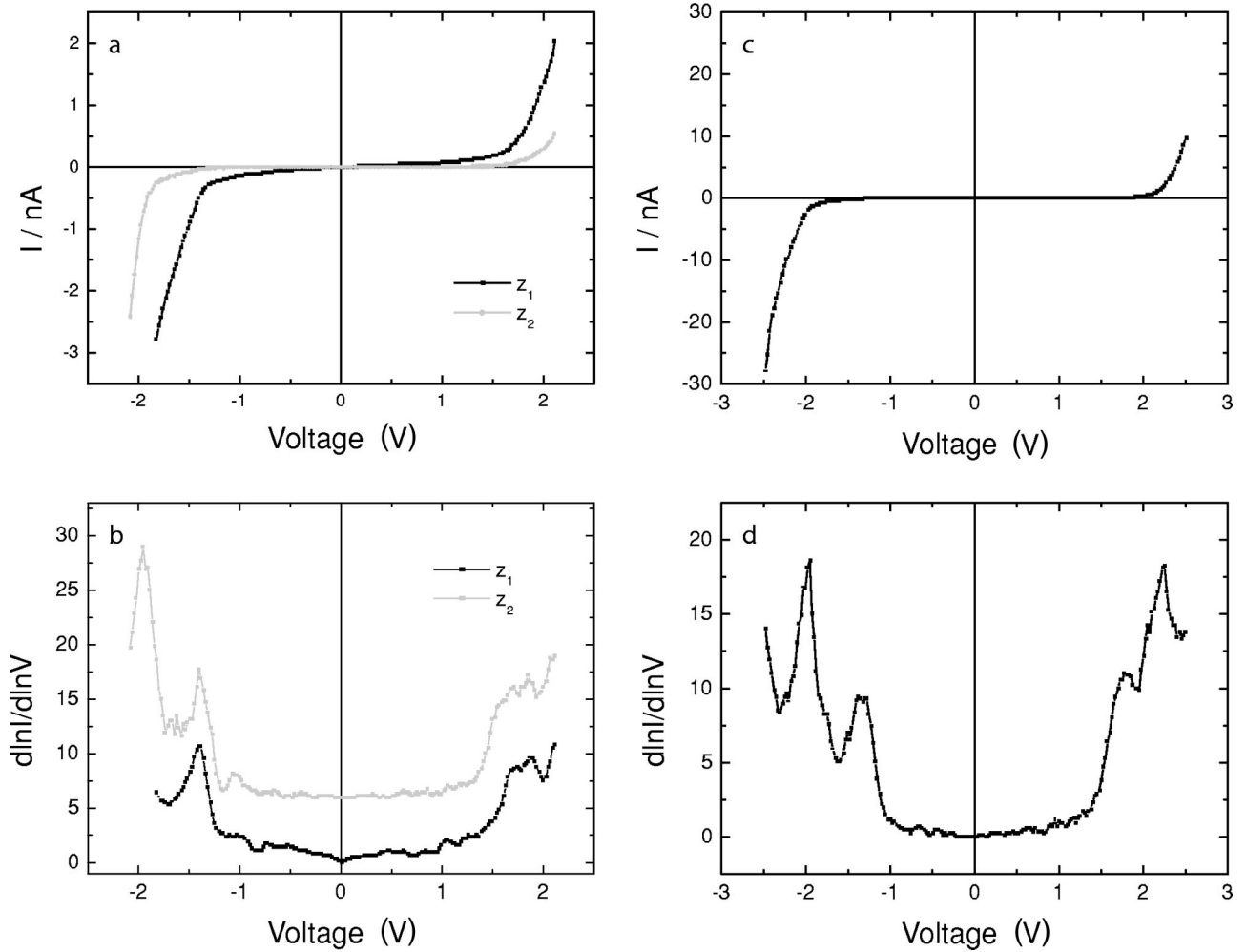


FIG. 3. (a)  $I$ - $V$  curves measured for two different (fixed) tip-sample distances at the same lateral position measured with a tungsten tip. The separation  $z_1$  (black curve) is determined by the tunneling parameters  $I=0.05$  nA and  $U=0.7$  V. The separation  $z_2$  (gray curve) was adjusted by changing the  $z$  piezo-voltage when the feedback loop was open. The distance  $z_2$  is nominally  $2.5$  Å larger than  $z_1$ . (b) Normalized differential conductance curves calculated from the data in (a). For better visibility the two curves in (b) are vertically shifted relative to each other by an additive constant of 5. (c)  $I$ - $V$  curve measured with a gold tip. The tunneling parameters were changed from  $0.05$  nA/ $0.7$  V to  $0.2$  nA/ $-1.5$  V before performing the STS measurements (i.e., with the feedback loop closed), thereby readjusting the tip-sample distance. (d) Normalized differential conductance curves calculated from the data in (c).

tip-sample separations. If there was a fraction of the bias voltage which is dropped at the molecule-substrate interface this fraction should change when increasing the tip-molecule separation. This change would then cause different peak positions for different tip-sample separations.

### III. THEORY AND COMPARISON WITH EXPERIMENT

#### A. Landauer formalism and density-functional-based tight-binding approach

According to the Landauer theory<sup>34,35</sup> the two-terminal linear-response conductance  $G$  of an object coupled to leads at zero temperature is proportional to the transmission probability  $T(E)$ , calculated at the equilibrium Fermi energy  $E_f$  of the whole system (leads plus object):

$$G = \frac{2e^2}{h} T(E_f). \quad (1)$$

The function  $T(E)$  is defined as:

$$T(E) = \text{Tr}(G_M^\dagger \Gamma_R G_M \Gamma_L). \quad (2)$$

The molecular Green function  $G_M$  has to be determined by solving a Dyson equation. In a nonorthogonal basis representation the latter takes the form

$$(zS_M - H_M - \Sigma_L(z) - \Sigma_R(z))G_M(z) = 1, \quad z = E + i0^+, \quad (3)$$

where  $H_M$  and  $S_M$  are the molecular Hamiltonian and overlap matrices. The self-energies  $\Sigma_\alpha(z)$ ,  $\alpha = L, R$  of the left ( $L$ ) and right ( $R$ ) leads appear after partitioning out the degrees of freedom of the electrodes<sup>36</sup> and contain information on the coupling between molecule and leads as well as on the electronic structure of the leads. They have the matrix representation,

$$\Sigma_{\alpha}(z) = (ES_{\alpha,M}^{\dagger} - V_{\alpha,M}^{\dagger})G_{\alpha}(z)(ES_{\alpha,M} - V_{\alpha,M}). \quad (4)$$

The matrices  $V_{\alpha,M}$  and  $S_{\alpha,M}$  are Hamiltonian and overlap matrix elements between molecular orbitals and lead orbitals and  $G_{\alpha}(z)$  is the Green function of the  $\alpha$ th semi-infinite lead. For simple electrode geometries, e.g., cubic lattices, analytical expressions for the Green function  $G_{\alpha}(z)$  can be found. For more complex geometries several numerical procedures have been developed. In this paper we use an approach based on decimation techniques.<sup>37,38</sup> The functions  $\Gamma_{\alpha}$  entering Eq. (2) are weighted surface densities of states of the leads and are defined as

$$\Gamma_{\alpha}(E) = i(\Sigma_{\alpha}(E + i0^{+}) - \Sigma_{\alpha}(E - i0^{-})). \quad (5)$$

In order to determine the object–lead coupling and the corresponding overlap matrices needed in Eq. (4), we follow a procedure introduced in Refs. 39 and 40 and consider a “supercluster” consisting of the molecule plus some relevant atoms belonging to the electrodes (the number of relevant atoms is basically determined by the range of the coupling matrices). From the Hamiltonian and overlap matrices of this “supercluster” the coupling matrices can be extracted. They are thus treated on the same footing as the Hamiltonian matrix of the object. In particular, changes in the topology of the lead–molecule interface are automatically included.

To solve Eq. (3) a characterization of the electronic structure of the molecule and the leads is necessary. We use a tight-binding-like scheme based on a linear-combination-of-atomic-(valence) orbitals (LCAO) ansatz, with matrix elements parametrized by DFT theory on the LDA level. This approach has been extensively applied to study the electronic and structural properties of a large variety of materials<sup>18,20,21</sup> and, recently, for investigating electronic transport properties of small sodium clusters<sup>41</sup> and carbon-based molecular junctions.<sup>42</sup> We therefore refer to the literature cited for more details of the method. The LCAO basis used in these calculations consists of the  $2s2p$  orbitals for carbon, the  $1s$  orbitals for hydrogen, and only the  $6s$  orbitals for gold. The inclusion of the  $5p5d$  orbitals for gold did not appreciably change the results, at least in the experimentally accessible region around the HOMO–LUMO gap.

Finally, the transmission function determines the current–voltage dependence via the equation (for zero temperature)

$$I(V) = \frac{2e}{h} \int_{E_F}^{E_F + eV} T(E) dE, \quad (6)$$

where an explicit voltage dependence of  $T(E)$  is neglected. By choosing the integration limits as in the above-given expression we are implicitly assuming that the applied potential is dropped entirely at the molecule–tip interface while the molecular potential is fixed with respect to the gold substrate, as discussed in Sec. II B.

From Eq. (6) the (normalized) differential conductance can be obtained as

$$\frac{d \ln I}{d \ln V} = \frac{2e^2 V}{hI} T(E_F + eV). \quad (7)$$

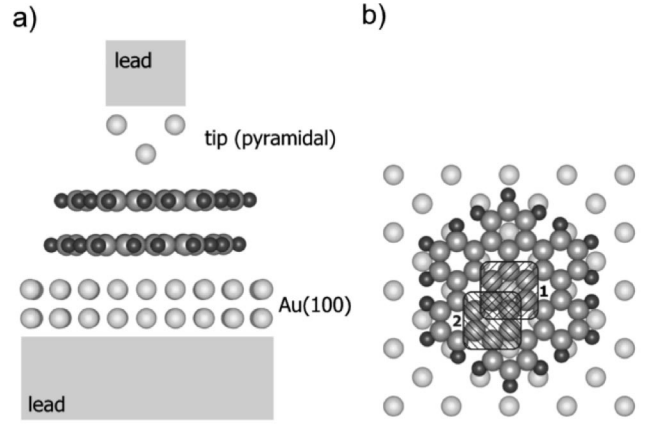


FIG. 4. (a) Side view of the tunnel junction showing the Au(100) substrate, two HBC molecules and a pyramidal tip. (b) Top view of HBC on Au(100). For simplicity only one monolayer is shown. Two squares (labeled 1 and 2) indicate the cross sections of the  $2 \times 2$  - STM tip at positions used in the transport calculations.

## B. Transport through a HBC double layer

The transport geometry we consider consists of a gold substrate with the (100) orientation and two monolayers of HBC (HBC<sub>2</sub>, each monolayer contains a single HBC molecule) on top of it at a distance of about 3.2 Å [see Fig. 4(a)].

The arrangement of the two HBC layers relative to each other cannot be derived from our STM and LEED measurements. There is also no HBC bulk plane with flat lying molecules from which this arrangement could be derived. On the other hand, molecular mechanics calculations have been performed for a single HBC molecule on HOPG.<sup>5,19</sup> These calculations revealed that the HBC molecule is arranged on the HOPG surface as if the carbon atoms of the molecule were belonging to a (second) graphite layer. Since the HBC molecule of the first layer resembles a cutoff of graphite, the two HBC monolayers in the calculations presented here were arranged in an  $A$ – $B$  stacking similar to the order of the basal planes in graphite.

The bond lengths of the isolated HBC<sub>2</sub> structure were first optimized using the DFT–LDA–LCAO approach mentioned previously combined with conjugated gradient techniques.<sup>20,21</sup> A layer-layer separation of 3.66 Å was found, indicating that the HBC layers are only very weakly coupled. For a single molecule the HOMO and the LUMO states are twofold degenerate.<sup>43</sup> Due to the interaction between the monolayers, this degeneracy will be partially lifted. Nevertheless, because of the weak interlayer coupling the splitting is almost negligible. The resulting gap between HOMO and LUMO was determined to be 2.62 eV, which is smaller than that suggested by optical absorption experiments where a value of around 2.8 eV was found for the first allowed optical transition.<sup>16</sup> In order to make an estimation for the HOMO–LUMO separation based on the optical absorption onset energy one would still have to add another 0.4 eV (Ref. 16) as the contribution of the exciton binding energy, resulting in a gap width of approximately 3.2 eV.

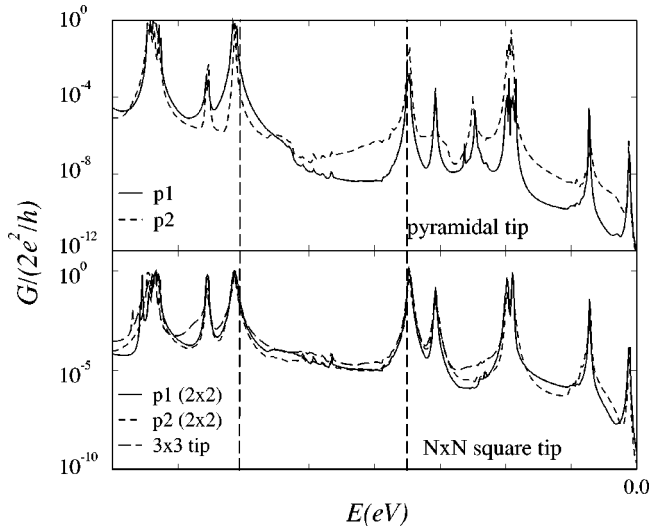


FIG. 5. Transmission probability  $T(E) = G/(2e^2/h)$  as a function of the injected electron energy for two monolayers of HBC on top of a Au(100) surface. The curves correspond to different STM tip geometries: pyramidal tips and  $2 \times 2$  square tips at positions 1 and 2 (see Fig. 4) above the molecule. Square tips with a larger cross section ( $3 \times 3$ ) did not change the results appreciably. Vertical dashed lines indicate the positions of the HOMO and LUMO levels of an isolated HBC double layer.

Although effects related to charge transfer (not included in our method) could further affect the calculated gap, we believe that the main source of the gap underestimation stems from the LDA treatment of the exchange and correlation functional. This is indeed a well-known effect of DFT-LDA.<sup>22,23</sup>

The gold substrate was modeled by a slab of 81 atoms in the stacking sequence  $ABAB \dots$  and with a finite cross section. The Au-lattice constant was chosen at 2.78 Å. The STM (gold)-tip was positioned vertically above the molecule. The distance between tip and HBC<sub>2</sub> was fixed at 2.50 Å. No further structural optimization of the combined substrate-HBC<sub>2</sub>-tip system was performed.

In order to check the sensitivity of our results to different tip structures, three simple tip geometries were investigated: (i) a  $2 \times 2$  square lattice, (ii) a pyramidal tip with one atom on top of the  $2 \times 2$  square lattice, and (iii) a  $3 \times 3$  square lattice. In Fig. 5 several transmission spectra for HBC<sub>2</sub> are shown. Different positions of the tip on the molecule were tested, but for a fixed tip geometry the transmission is quite insensitive to the (lateral) tip position, at least concerning the energy region around the HOMO-LUMO gap (see Fig. 5). Therefore, only two different positions are discussed in the following (schematically shown in Fig. 4). Moreover, a rotation of the molecule around an axis perpendicular to the Au(100) surface had only a minor influence on  $T(E)$ . For all scattering geometries studied the shift of the molecular HOMO and LUMO states by coupling to the substrate and the STM tip is almost negligible, which is expected because of the relative large molecule-substrate and molecule-tip separations.

The basic feature found for a pyramidal tip geometry is that the LUMO resonance shows a transmission about one order of magnitude smaller than the HOMO. The HOMO resonance is narrower for position 2, probably due to the low charge density at the center of the rings. Structures showing up within the molecular HOMO-LUMO gap as small spikes are gold states resulting from finite-size effects in modeling the gold surface.

In contrast, for a  $2 \times 2$  square tip both HOMO and LUMO resonances show almost ideal transmission. A tip with a larger cross section ( $3 \times 3$ ) does not further influence appreciably the conductance spectrum (Fig. 5). This behavior apparently differs from the results reported in Ref. 44 where  $T(E = E_{\text{LUMO}})$  is about two orders of magnitude smaller than  $T(E = E_{\text{HOMO}})$  for a large square surface. The differences may be related to the approximations used in the two different approaches but also to differences in the geometrical structure and symmetry of the transport setup (metallic electrodes plus molecule) which could lead to different coupling strengths of the molecular resonances to the electronic states of the electrodes and thus to different contributions to the transmission amplitudes. In order to make connection with the STS experiments the normalized differential conductance  $d \ln I/d \ln V$  was computed. A central point here is the determination of the Fermi energy. For this an accurate electronic band structure of the substrate and the tip as well as the charge transfer at the molecule-lead interface should be known. As suggested by Datta *et al.*<sup>39</sup> the Fermi energy might be used as a fit parameter. However, to obtain a first approximation, we used the extended cluster defined at the end of Sec. III A. The Hamiltonian and overlap matrices were constructed and the associated eigenvalue problem was solved. After appropriately populating the electronic states, the obtained HOMO level at about  $-4.74$  eV was taken as an approximation to the Fermi energy. This is too close to the vacuum level compared to the experimentally known value for the work function of the bare Au(100) surface of  $-5.2$  eV.<sup>45</sup> However, due to the existence of a surface dipole, the workfunction of a HBC film on gold would provide a better reference point for the (calculated) Fermi energy of the system. The latter value was determined as  $-4.5$  eV.<sup>16</sup> Therefore, the calculated value is in fact slightly too far from the vacuum level (approximately by 0.25 eV).

In Fig. 6 the voltage dependence of the normalized differential conductance is compared to the experimental data for two different tip geometries. We are mainly interested in the peak positions. Peak widths are determined in the theory by the coupling to the electrodes (which is rather weak), while in the experiment different surroundings of the molecules and excitation of vibronic states as well as finite temperatures can induce additional broadening. Therefore, we have convoluted the theoretical spectra with Gauss functions with a full width at half maximum value of 0.1 eV.

There is a nearly perfect agreement between the theoretical and experimental values of the HOMO peak position (at  $-1.4$  V), in particular for the case of the pyramidal tip. For the other features in the spectra there is no such close correlation between the experimental and calculated data.

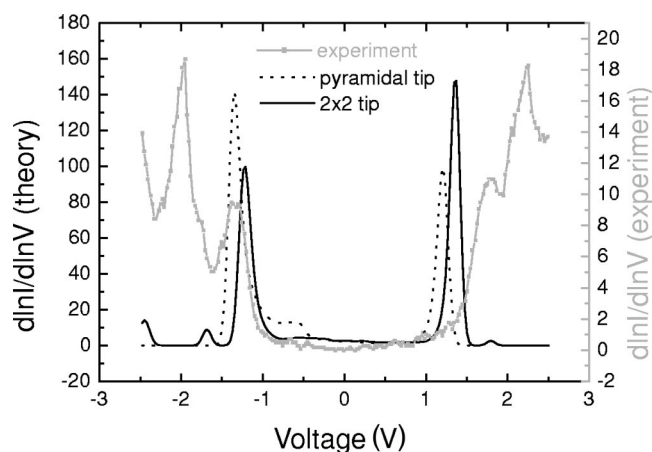


FIG. 6. Comparison of the experimental (gray) differential conductance with the theoretical spectra showing results for two different tip geometries: pyramidal tip (dashed line) and  $2 \times 2$  square tip (full line). The theoretical spectra have been convoluted with Gaussian functions of width 0.1 eV. Note that an even better agreement could be achieved if the benchmark of the theoretical energy scale would be adjusted in accordance with the experimental value (see the text), which would mean an additional shift of 0.25 eV to more positive values.

As mentioned previously, the HOMO–LUMO gap is strongly underestimated within the LDA approach. In order to compensate for this effect, a linear scaling procedure for the occupied and unoccupied Kohn–Sham energy levels has been recently proposed.<sup>24</sup> In Fig. 7 we compare the experimental data with the scaled normalized differential conductance spectrum for the case of the  $2 \times 2$  square tip geometry. By choosing a scaling parameter value of 1.18 a reasonable agreement in the peak positions was achieved when comparing the calculated and experimentally obtained values. This allows one to relate the first two peaks for negative (positive) bias to resonant tunneling through the first and second filled (empty) molecular states. For an easier comparison of the peak positions the calculated curve was plotted on a logarithmic scale in Fig. 7 while the experimental data are plotted on a linear scale. One should keep in mind, however, that other effects not included in the theoretical treatment may introduce additional corrections to the positions and intensities of the molecular resonances. Such are, e.g., electric fields induced in the molecule in the nonlinear voltage region, i.e. for applied bias larger than the HOMO–LUMO gap. This would require a self-consistent calculation of the potential distribution in the molecular region, which introduces an explicit voltage dependence in the transmission function. This lies, however, beyond the scope of this paper.

#### IV. SUMMARY/CONCLUSION

We have presented scanning tunneling spectroscopy results measured on a highly ordered film of the planar organic molecule hexa-*peri*-hexabenzocoronene deposited on Au(100) substrates by means of organic molecular beam ep-

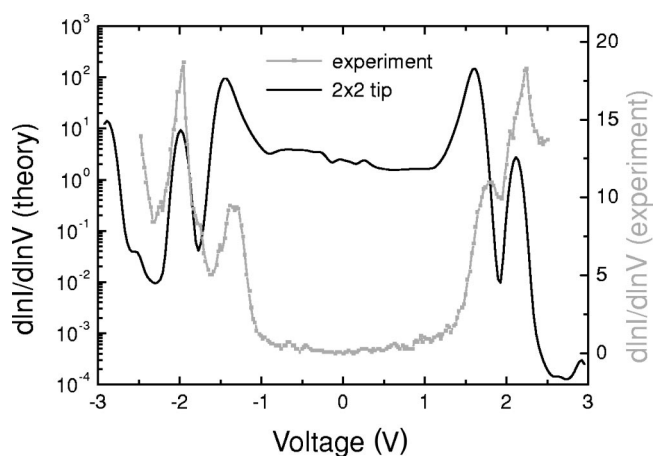


FIG. 7. Comparison of the experimental (gray) differential conductance with the theoretical spectra. The voltage axis for the calculated conductance has been rescaled by a factor of 1.18. Note that the calculated conductance has been plotted on a logarithmic scale (see the text). The theoretical spectra have been convoluted with Gaussian functions of width 0.1 eV.

itaxy. The normalized differential conductance curves calculated from the measured  $I$ – $V$  data reveal four peaks within the extended accessible voltage range at +2.2, +1.8, –1.4, and –2.0 V, which are attributed to resonant tunneling via LUMO+1, LUMO, HOMO, and HOMO–1, respectively. Moreover, identical peak positions are found for different tip–sample separations and for different tip materials (tungsten and gold), providing evidence that the above-mentioned values are really characterizing properties of the molecular film on gold.

A theoretical model for the electronic conductance of HBC films adsorbed on the Au(100) surface was outlined. The theoretical approach is based on a combination of the Landauer transport formalism with an approximative density-functional scheme. The calculated transmission probability does not show a significant dependence on the tip position. The normalized differential conductance  $d \ln I/d \ln V$  was computed from the transmission probability and compared to the experimental data. A scaling parameter was used to compensate for the underestimation of the electronic HOMO–LUMO gap within the local-density approximation. Using the scaled conductance spectrum for a  $2 \times 2$  square tip geometry a satisfactory agreement with the experimental data was obtained.

#### ACKNOWLEDGMENTS

This research was supported by the “Deutsche Forschungsgemeinschaft” through FOR335 “Nanostrukturierte Funktionselemente in makroskopischen Systemen.” The authors acknowledge the group of K. Müllen at the MPI für Polymerforschung in Mainz for providing the HBC. R.G. thanks G. Seifert for useful comments. The authors are very grateful to K. Leo for his interest and support of these studies.

- \*Electronic mail: toerker@iapp.de; URL: www.iapp.de  
 †URL: www.physik.tu-dresden.de/frank
- <sup>1</sup>T.J.Schuerlein, A. Schmidt, P.A. Lee, K.W. Nebesny, and N.R. Armstrong, *Jpn. J. Appl. Phys., Part 1* **34**, 3837 (1995).
  - <sup>2</sup>C. Seidel, J. Poppensieker, and H. Fuchs, *Surf. Sci.* **408**, 223 (1998).
  - <sup>3</sup>K. Glöckler, C. Seidel, A. Soukopp, M. Sokolowski, E. Umbach, M. Böhringer, R. Berndt, and W. Schneider, *Surf. Sci.* **405**, 1 (1998).
  - <sup>4</sup>T. Fritz, *Molecular Architecture in Heteroepitaxially Grown Organic Thin Films* (Wissenschaftlicher Fachverlag, Dresden, 1999).
  - <sup>5</sup>T. Schmitz-Hübsch, F. Sellam, R. Staub, M. Törker, T. Fritz, C. Kübel, K. Müllen, and K. Leo, *Surf. Sci.* **445**, 358 (2000).
  - <sup>6</sup>S. Mannsfeld, M. Toerker, T. Schmitz-Hübsch, F. Sellam, T. Fritz, and K. Leo, *Organic Electronics* **2**, 121 (2001).
  - <sup>7</sup>X. Zhou, J. Blochwitz, M. Pfeiffer, A. Nollau, T. Fritz, and K. Leo, *Advanced Functional Materials* **11**(4), 310 (2001).
  - <sup>8</sup>L. Scudiero, D.E. Barlow, U. Mazur, and K.W. Hipps, *J. Am. Chem. Soc.* **123**, 4073 (2001).
  - <sup>9</sup>S. Hong, R. Reifengerger, W. Tian, S. Datta, J. Henderson, and C.P. Kubiak, *Superlattices Microstruct.* **28**, 289 (2000).
  - <sup>10</sup>T. David, J.K. Gimzewski, D. Purdie, B. Reihl, and R.R. Schlittler, *Phys. Rev. B* **50**, 5810 (1994).
  - <sup>11</sup>F. Dietz, N. Tyutyulkov, G. Madjarova, and K. Müllen, *J. Phys. Chem. B* **104**, 1746 (2000).
  - <sup>12</sup>A.V. de Craats, J. Warman, A. Fechtenkötters, J.D. Brandt, M. Harbison, and K. Müllen, *Adv. Mater.* **11**, 1469 (1999).
  - <sup>13</sup>F. Sellam, T. Schmitz-Hübsch, M. Toerker, S. Mannsfeld, H. Proehl, T. Fritz, K. Leo, Ch. Simpson, and K. Müllen, *Surf. Sci.* **478**, 113 (2001).
  - <sup>14</sup>U. Zimmermann and N. Karl, *Surf. Sci.* **268**, 296 (1992).
  - <sup>15</sup>N. Karl and C. Günther, *Cryst. Res. Technol.* **34**, 243 (1999).
  - <sup>16</sup>H. Proehl, M. Toerker, T. Fritz, F. Sellam, K. Leo, Ch. Simpson, and K. Müllen, *Phys. Rev. B* **63**, 205409 (2001).
  - <sup>17</sup>A. Stabel, P. Herwig, K. Müllen, and J. Rabe, *Angew. Chem.* **107**, 1768 (1995).
  - <sup>18</sup>D. Porezag, Th. Frauenheim, and Th. Köhler, *Phys. Rev. B* **51**, 12 947 (1995).
  - <sup>19</sup>T. Schmitz-Hübsch, Ph.D. thesis, T. U. Dresden, Germany (unpublished).
  - <sup>20</sup>O. Knosppe, R. Schmidt, and G. Seifert, in *Advances in Classical Trajectory Methods*, edited by W. L. Hase (JAI Press, Stayford, 1999), Vol. 4, p. 153.
  - <sup>21</sup>*Computer Simulation of Materials at Atomic Level*, edited by P. Deak, Th. Frauenheim, and M. Pederson (Wiley-VCH, Berlin, 2000).
  - <sup>22</sup>M. Rohlfing, P. Krüger, and J. Pollmann, *Phys. Rev. B* **48**, 17 791 (1993).
  - <sup>23</sup>M. Springborg, *Methods of Electronic-Structure Calculations*, Wiley Series in Theoretical Chemistry (Wiley, New York, 2000).
  - <sup>24</sup>R. Stowasser and R. Hoffmann, *J. Am. Chem. Soc.* **121**, 3414 (1999).
  - <sup>25</sup>R. Feenstra, J. Stroscio, and A. Fein, *Surf. Sci.* **181**, 295 (1987).
  - <sup>26</sup>M. Toerker, T. Fritz, H. Proehl, F. Sellam, and K. Leo, *Surf. Sci.* **491**, 255 (2001).
  - <sup>27</sup>R. Rinaldi, R. Cingolani, K.M. Jones, A.A. Baski, and H. Morkoc, *Phys. Rev. B* **63**, 075311 (2001).
  - <sup>28</sup>R. Strohmaier, C. Ludwig, J. Petersen, B. Gompf, and W. Eisenmenger, *Surf. Sci.* **351**, 292 (1996).
  - <sup>29</sup>P.G. Collins, J.C. Grossmann, M. Côté, M. Ishigami, C. Piskoti, S.G. Louie, M.L. Cohen, and A. Zettl, *Phys. Rev. Lett.* **82**, 165 (1999).
  - <sup>30</sup>M. Prietsch, A. Samsavar, and R. Ludeke, *Phys. Rev. B* **43**, 11 850 (1991).
  - <sup>31</sup>H. Sumi, *J. Phys. Chem. B* **102**, 1833 (1998).
  - <sup>32</sup>W. Han, E.N. Durantini, T.A. Moore, A.L. Moore, D. Gust, P. Rez, G. Leatherman, G.R. Seely, N. Tao, S.M. Lindsay, *J. Phys. Chem. B* **101**, 10 719 (1997).
  - <sup>33</sup>S. Datta, W. Tian, S. Hong, R. Reifenberger, J.I. Henderson, and C.P. Kubiak, *Phys. Rev. Lett.* **79**, 2530 (1997).
  - <sup>34</sup>S. Datta, *Electronic Transport in Mesoscopic Systems* (Cambridge University Press, Cambridge, 1995).
  - <sup>35</sup>A. Nitzan, *Annu. Rev. Phys. Chem.* **52**, 681 (2001).
  - <sup>36</sup>S. Priyadarshi, S. Skourtis, S.M. Risser, and D.N. Beratan, *J. Chem. Phys.* **104**, 9473 (1996).
  - <sup>37</sup>M.P. Lopez Sancho, J.M. Lopez Sancho, and J. Rubio, *J. Phys. F: Met. Phys.* **14**, 1205 (1984).
  - <sup>38</sup>This technique is based on the concept of a principal layer. For defining a principal layer atomic planes are collected in such a way that only nearest-neighbor interactions between principal layers exist, thus reducing the system to an effective nearest-neighbor tight-binding problem. Thus, for a Au(100) surface with the stacking sequence ABAB... a principal layer contains two atomic planes. Since the coupling matrix elements  $V_{\alpha,M}$  in Eq. (4) are short-ranged, they will eliminate all contributions coming from principal layers other than the first one, the surface principal layer. Hence, only the Green function of this layer (surface Green function) will be needed in these calculations.
  - <sup>39</sup>W. Tian, S. Datta, S. Hong, R. Reifenberger, J.I. Henderson, and C.P. Kubiak, *J. Chem. Phys.* **109**, 2874 (1998).
  - <sup>40</sup>S.N. Yaliraki, A.E. Roitberg, C. Gonzalez, V. Mujica, and M. Ratner, *J. Chem. Phys.* **111**, 6997 (1999).
  - <sup>41</sup>R. Gutierrez, F. Grossmann, O. Knosppe, and R. Schmidt, *Phys. Rev. A* **64**, 013202 (2001).
  - <sup>42</sup>R. Gutierrez, G. Fagas, G. Cuniberti, F. Grossmann, K. Richter, and R. Schmidt, *Phys. Rev. B* **65**, 113410 (2002).
  - <sup>43</sup>Within DFT or DFT-based methods the electronic eigenvalues are regarded as devoid of any physical significance (with the exception of the HOMO). Nevertheless, in practical calculations, it was pointed out that they are indeed suitable for chemical applications [see, for instance, W. Koch and M. C. Holthausen, *A Chemist's Guide to Density Functional Theory* (Wiley-VCH, Weinheim, 2001), and references therein], in particular, for connecting the experimental ionization potentials with the Kohn-Sham eigenvalues, scaled in an appropriated way (Ref. 24). In this sense, we speak of HOMO and LUMO when comparing our theoretical calculations with the experimental data.
  - <sup>44</sup>M. Paulsson and S. Stafström, *J. Phys.: Condens. Matter* **12**, 9433 (2000).
  - <sup>45</sup>G.V. Hansson and S.A. Flodström, *Phys. Rev. B* **18**, 1572 (1978).